Water ice clouds over the Martian tropics during northern summer

N. G. Heavens,[1,2] J. L. Benson,[3] D. M. Kass,[3] A. Kleinböhl,[3] W. A. Abdou,[3] D. J. McCleese,[3] M. I. Richardson,[4] J. T. Schofield,[3] J. H. Shirley,[3] and P. M. Wolkenberg[3]

[1] Atmospheric models suggest that infrared heating due to water ice clouds over the tropics of Mars during early northern summer has a significant impact on the thermal structure of the tropics at cloud level and of the middle atmosphere near the south pole. Retrievals from limb observations by the Mars Climate Sounder on Mars Reconnaissance Orbiter during early northern summer show that water ice clouds over the northern tropics are thinner and higher than in published model results. Later in this season, the latitudinal extent, apparent mass mixing ratio (and infrared heating rate), and altitude of nighttime tropical clouds significantly increase, reaching a maximum just before northern fall equinox. Published model results do not show this transition. By underestimating the altitude at which water ice clouds form, models also may underestimate the intensity of the meridional circulation at higher altitudes in the tropics during northern summer. **Citation:** Heavens, N. G., J. L. Benson, D. M. Kass, A. Kleinböhl, W. A. Abdou, D. J. McCleese, M. I. Richardson, J. T. Schofield, J. H. Shirley, and P. M. Wolkenberg (2010), Water ice clouds over the Martian tropics during northern summer, *Geophys. Res. Lett.*, *37*, L18202, doi:10.1029/2010GL044610.

1. Introduction

[2] Water ice clouds are a common feature of the Martian atmosphere. The most optically thick of these clouds are observed on the edge of the winter polar caps and near high volcanoes throughout much of the year and in the tropics during northern spring and summer, during which the average visible optical depth in the tropics reaches ~0.4 and clouds can have much greater optical depths locally [e.g., *Wang and Ingersoll*, 2002; *Smith*, 2004]. Water ice clouds reflect incoming solar radiation and absorb and re-emit thermal infrared radiation upwelling from the surface in a thin, infrared-transparent atmosphere. Thus, they affect the energy budget of both the atmosphere and the surface in their vicinity significantly [*Hinson and Wilson*, 2004; *Wilson et al.*, 2007], and atmospheric models suggest they have a substantial effect on the thermal structure globally.

[3] *Wilson et al.* [2008] found a significant discrepancy between temperatures during early northern summer simulated by a control run of the UK Mars general circulation model (MGCM) and by a model run assimilating retrievals of temperature and dust column opacity from the Thermal Emission Spectrometer (TES) on Mars Global Surveyor (MGS). *Wilson et al.* [2008] attribute this discrepancy to the radiative effects of water ice clouds, which were not included in the UK MGCM simulations, and find that simulating clouds in the Geophysical Fluid Dynamics Laboratory (GFDL) MGCM results in 5—10 K warmer temperatures in the tropics (at the latitude and just above the altitude of the highest zonal average water ice mass mixing ratio) and up to 20 K warmer temperatures at 10 Pa at 60°S. Thus, water ice clouds may affect the atmospheric thermal structure directly through radiative heating/cooling and indirectly through dynamical processes.

[4] The vast majority of water ice cloud observations on Mars are of dayside column opacity (or roughly equivalent nadir imagery), which constrains the effect of water ice clouds on the shortwave heating of the surface. Vertical profiling, however, is necessary to constrain the primarily longwave radiative heating/cooling of the atmosphere due to clouds, since the same column opacity could be due to either a shallow ground fog or a vertically extended haze, but the radiative heating rate profiles, downwelling longwave radiation at the surface, and dynamical effects in these two cases may be very different. Retrievals from limb observations by the Mars Climate Sounder (MCS) on Mars Reconnaissance Orbiter (MRO) now provide a rich dataset for exploring the vertical distribution of water ice clouds [*McCleese et al.*, 2007; *Kleinböhl et al.*, 2009]. They already have been used to study south polar hood clouds [*Benson et al.*, 2010] and the effects of the thermal tides on clouds [*Lee et al.*, 2009]. Here we use MCS retrievals to investigate the spatial distribution of water ice clouds during northern summer and early northern fall, a period of transition in visible imagery from widespread tropical cloudiness (during the period simulated by *Wilson et al.* [2008]) to the tropics being relatively clear of water ice clouds [*Wang and Ingersoll*, 2002].

2. Data and Methods

[5] Atmospheric retrievals from MCS observations provide vertical profiles of pressure, p, (Pa), temperature, T, (K), water ice opacity, i.e., fractional extinction due to water ice per unit height, $d_z\tau$, (km^{-1}) at 843 cm^{-1}, and dust opacity (km^{-1}) at 463 cm^{-1}. The retrieved profiles and the hydrostatic equation can be used to estimate the surface pressure. *Kleinböhl et al.* [2009] describe the retrieval algorithm in far

---

[1]Division of the Geological and Planetary Sciences, California Institute of Technology, Pasadena, California, USA.
[2]Now at Department of Earth and Atmospheric Sciences, Cornell University, Ithaca, New York, USA.
[3]Jet Propulsion Laboratory, California Institute of Technology, Pasadena, California, USA.
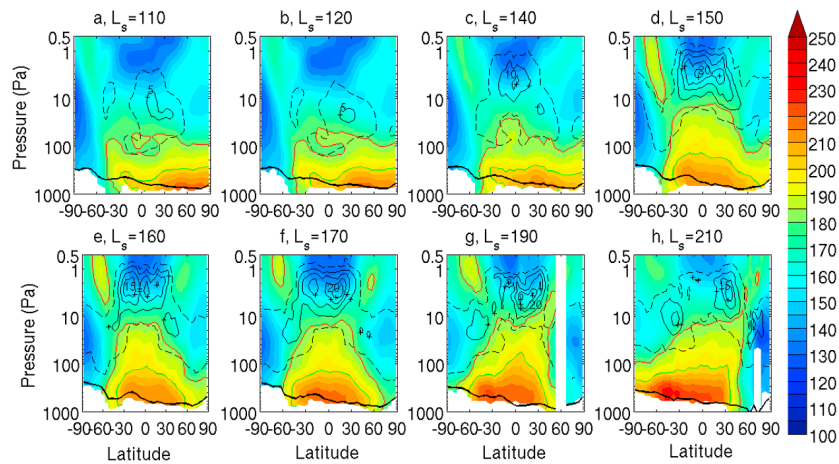[4]Ashima Research, Pasadena, California, USA.

Figure 1. Nightside zonal average temperature (K) (shaded contours) and q_{ice} (ppm) (contours) for selected (a–h) L_s bins during MY 29 as labeled. The black dashed contour indicates 1 ppm. The black contours with crosses mark 5 ppm intervals, and the maximum contour is labeled. The green and red solid contours mark the 200 K and 180 K isotherms respectively. The thick black contour indicates the zonal average surface pressure.

greater detail than we can here and evaluates its success under different observational conditions. For $d_z\tau > 10^{-5}$ km^{-1}, the estimated uncertainty in $d_z\tau$ is typically ~5%. The retrievals analyzed here use an advanced version of the retrieval algorithm that includes a simple scattering approximation in the radiative transfer as presented by A. Kleinböhl et al. (Mars Climate Sounder limb retrievals of dust and water ice using scattering radiative transfer: Implications for particle size, Mars Dust Cycle Workshop, NASA Ames Research Center, Mountain View, California, 15–17 September 2009).

[6] If the effective radius (r_{eff}) and extinction coefficient (Q_{ext}) of the particle size distribution and the density of water ice (ρ_{ice}) are known, the mass mixing ratio of water ice (q_{ice}) can be derived from any individual retrieval (spherical particles of pure water ice are assumed in this case):

$$q_{ice} = \frac{4}{3} \frac{\rho_{ice}}{Q_{ext}} \frac{d_z\tau}{\rho} r_{eff} \qquad (1)$$

where ρ is the atmospheric density. We assume $\rho_{ice} = 900$ kg m^{-3} and use the same assumptions for r_{eff} (1.41 μm) and Q_{ext} (0.773) as in the retrieval algorithm. While such a construction is useful for comparison with model output and so will be adopted for the data analysis, it is only as exact as its assumptions are correct. For instance, if the grain size of water ice particles is much larger than assumed, r_{eff}/Q_{ext} (and q_{ice}) could increase by a factor of 2. If water ice particles nucleate around dust particles, ρ_{ice} will depend on the thickness of the water ice layer coating the dust particle.

[7] The infrared heating rate due to water ice using the optically thin, plane-parallel, and non-scattering approximations for emission of the surface at temperature T_s and re-emission by the cloud at T_e is:

$$\frac{dT}{dt} = \frac{\frac{d_z\tau}{\rho}\pi \int\limits_0^\infty \frac{Q_{ext,\nu}}{Q_{ext,MCS}}(1 - \omega_\nu)[B_\nu(T_s) - 2B_\nu(T_e)]d\nu}{c_p} \qquad (2)$$

where ν denotes frequency, MCS denotes the channel in which MCS retrieves ice, ω_ν is the single scattering albedo,

$B_\nu(T)$ is the Planck function, and c_p is the heat capacity of the atmosphere. Thus, the heating rate is proportional to the density-scaled opacity, $\frac{d_z\tau}{\rho}$, which can be directly calculated from the retrievals, is proportional to q_{ice} as we calculate it, and is affected by the uncertainty in the properties of water ice (and dust) only to the extent that uncertainty affects relative attribution of opacity to dust and water ice in the retrieval algorithm [*Kleinböhl et al.*, 2009].

[8] For zonal averaging, the retrievals are separated into "dayside" (9:00—21:00 LST) and "nightside" (21:00—9:00 LST) bins and further binned in 36 (5° resolution) mean latitudinal bins, 64 (5.625° resolution) mean longitudinal bins, and L_s bins at 5° resolution. Away from the poles, MCS normally observes ~3:00 and ~15:00 LST. Mean latitude and longitude refer to the coordinates at the tangent point observed by the center of the MCS detector array at ~40 km above the surface. Opacity at pressures lower than the lowest pressure at which opacity is reported is set to 0 to minimize the impact on the zonal average of rare hazes detached from the bulk of the cloud.

3. Results

[9] Figures 1a–1h show nightside zonal average temperature (K) and q_{ice} for selected L_s bins during northern summer and fall of Mars Year (MY) 29 (2008–2009) (by the convention of *Clancy et al.* [2000]). (The latitude/longitude bins that contribute to the zonal averages in Figure 1 are mapped in Figure S1 of the auxiliary material.)[1] Sampling of longitudinal bins is good in early summer and degrades as the summer progresses. Therefore, averages in some latitudinal/L_s bins are based on a relatively small number of retrievals. We focus on nightside profiles, because sampling is usually better during the night.

[10] In early summer, the highest zonal average nightside q_{ice} is 5 parts per million (ppm) over the northern tropics at ~20 Pa (Figures 1a and 1b). By L_s=140°, a layer of higher
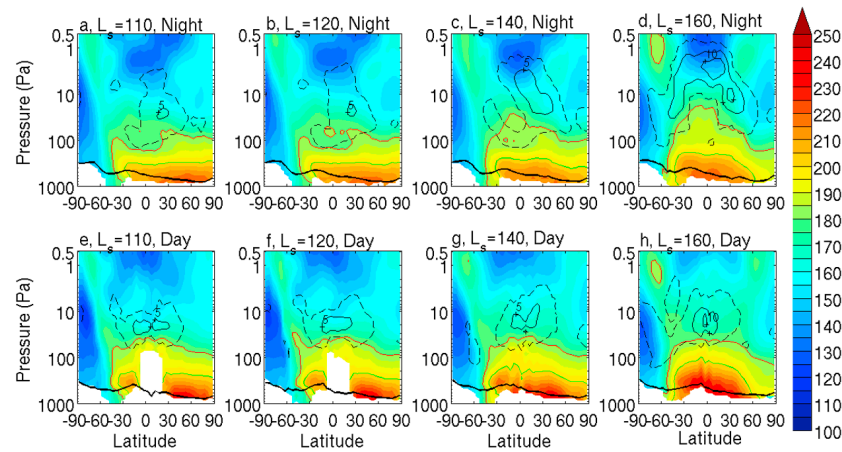
Figure 2. Zonal average temperature (K) (shaded contours) and q_{ice} (ppm) (contours) for selected (a–h) L_s bins during MY 28 for dayside or nightside as indicated by the labels at the top of each panel. The meaning of the color contours and other markings is the same as in Figure 1.

q_{ice} stretches across the tropics at ~4 Pa (Figure 1c), and this layer increases in q_{ice} (up to 20 ppm) throughout late summer as secondary maxima in q_{ice} of 5 ppm become apparent near 45°N and S at ~ 10–20 Pa (Figures 1e and 1f). The layer of high q_{ice} at ~4 Pa over the tropics begins to dissipate in early northern fall. Figures 2a and 2d show a similar transition in the distribution of water ice at night during the course of the summer of MY 28, during which longitudinal sampling is somewhat better later in the summer than during MY 29 (Figures S2a–S2d). On the dayside, a tropically symmetric layer of water ice with q_{ice}=5—10 ppm is observed at ~20 Pa throughout northern summer (Figures 2e–2h), though sampling is poor (Figures S2e–S2h).

[11] Figures 3a and 3b show longitudinal cross-sections of q_{ice} from a narrow latitude band centered on the northern tropic and intersecting Lycus Sulci and the Elysium Montes. In the example from early summer of MY 29 (Figure 3a), there is a layer of high q_{ice} at ~20 Pa, which does not vary much in q_{ice} or pressure level with longitude, even at longitudes that cross significant topography. This layer is vertically resolved by the retrievals. In the example from late summer of MY 28 (Figure 3b), q_{ice} is more longitudinally variable. There are layers of water ice with similar values of q_{ice} and at similar pressure levels as those in early summer, but there is also a layer at ~3 Pa with q_{ice} up to 30 ppm.

[12] Figures 3c and 3d show longitudinal cross-sections of q_{ice} from a narrow latitude band at the equator that intersects the Tharsis Montes. In the example from early summer of MY 29 (Figure 3c), there are a couple of vertically resolved layers of q_{ice} of ~ 10 ppm at ~ 20 Pa. One layer is near and just east of the Tharsis Montes between 120°—80°W, while the other is between 0°—60° E. The longitudinal sampling is not as complete as in Figure 3a, but the thick water ice clouds seem somewhat more scattered. In the example from late summer (Figure 3d), scattered cloudiness is now at a pressure level between 2 and 10 Pa, while the q_{ice} of the thickest layers is a factor of 3 greater.

4. Discussion

[13] The tropical water ice distribution in early northern summer and the course of its evolution during northern

summer do not appear to be captured well by published models. *Richardson et al.* [2002], *Montmessin et al.* [2004], *Wilson et al.* [2008], and *Nelli et al.* [2009] all predict that the thickest clouds in early summer are mostly in the northern tropics at ~100 to 300 Pa (perhaps up to 50 Pa as in the work by *Montmessin et al.* [2004]), a significantly lower level in the atmosphere than where they are observed. (The first three studies present diurnal averages, while *Nelli et al.* [2009] present longitudinal cross-sections for night.) The simulated q_{ice} for these clouds in these published models is ~5 times higher than observed, a discrepancy too great to be explained by the grain size assumption used in equation (1). *Richardson et al.* [2002] simulate a transition in the tropical water ice distribution during northern summer, but it is a transition from a tropically symmetric layer at a pressure level of ~200 Pa at L_s=110° to a thinner layer mainly over the northern tropics at a pressure level of ~100 Pa at L_s=150°. Both of these layers are at much higher pressures than observed.

[14] Part of the discrepancy in the pressure level of clouds may be due to the limited vertical range of the retrievals, which because MCS retrievals are primarily based on limb observations, is dependent on altitude above the surface rather than pressure. Retrieval near the surface is inhibited by potentially large opacity in the instrument line-of-sight and substantial contributions of emission from the surface in the measured radiances, so the retrievals generally are cut off below ~5 to 15 km above the surface (see Figure 3 for relevant pressure information).Thus, the retrieved profiles will miss clouds near the surface, especially in the vicinity of topography, that could contribute high q_{ice} to model simulations at some pressure levels. In Figure 3c, for instance, the retrievals near the Tharsis Montes stop at ~100 Pa. Yet modeling by both *Hinson and Wilson* [2004] and *Spiga and Forget* [2009] predict that thick clouds above Tharsis develop at higher pressures (and lower altitudes).

[15] This bias against "seeing" low clouds is likely intrinsic to limb observations in the thermal infrared at this season. These results agree well with TES limb retrieval results presented by McConnochie and Smith (Vertically Resolved Water Ice Aerosols Opacity From Mars Global Surveyor Thermal Emission Spectrometer (TES) Limb Sounding, Mars
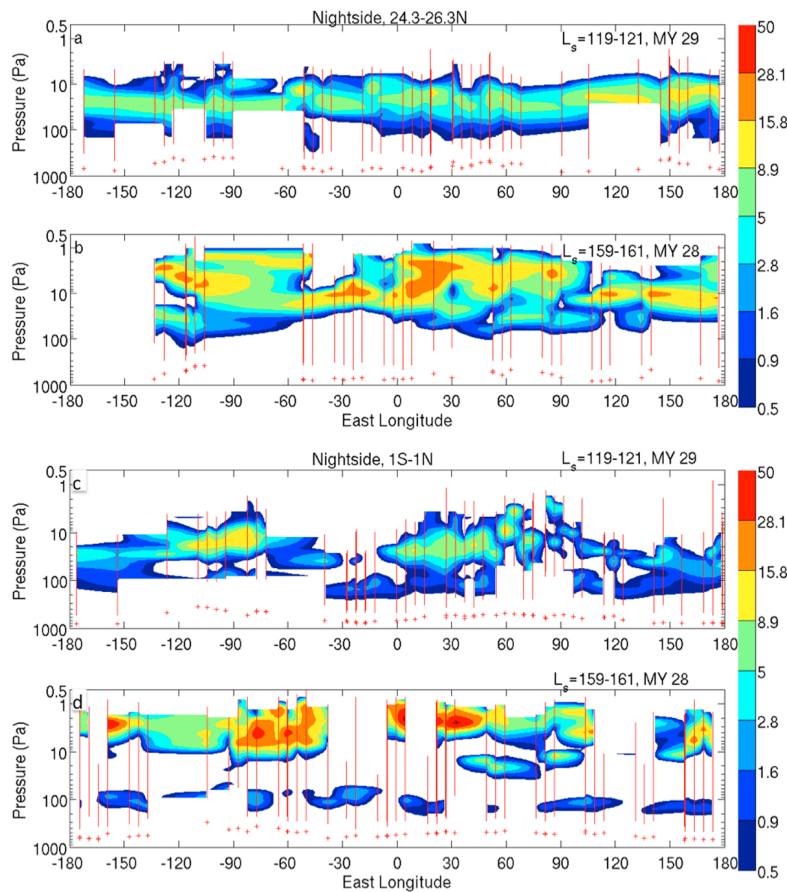
Figure 3. (a–d) Nightside q_{ice} (ppm) for four longitudinal cross-sections interpolating retrievals from a narrow range of latitude and L_s. See the labels on the figure itself for details. The red lines mark the mean longitude and vertical extent of the simultaneous retrieval of water ice and temperature in the cross-section. The red crosses mark the estimated surface pressure for each retrieval. Temperature retrieval may use nadir or off-nadir information and so may occur at a higher pressure level than water ice retrieval without implying anything about water ice opacity. Temperature retrieval, however, normally continues at much lower pressure levels than water ice is retrieved, generally indicating that the radiance due to water ice opacity has fallen below the instrument noise level. Note the logarithmic scale. The data in Figures 3a and 3c is from a different year than the data in Figures 3b and 3d, so while the seasonal evolution in zonal average q_{ice} is similar between MY 28 and 29, differences between Figures 3a and 3b or between Figures 3c and 3d may reflect both seasonal evolution and interannual variability.

Water Cycle Workshop, CNRS, 21–23 April 2008, Paris, France). But the vertical range bias cannot explain the entirety of the difference between the models and the observed water ice distribution. The vertical range of the retrievals reaches pressures as high as 300 Pa over most of the planet along the northern tropic (Figure 3a). Based on the simulations of *Wilson et al.* [2008], we would expect to resolve a layer of cloud with q_{ice} of 10—20 ppm centered at 100 Pa, but such a layer is not observed. In addition, the model whose q_{ice} output is gridded sufficiently finely to make a comparison, *Richardson et al.* [2002], predict that zonal average q_{ice} at pressures lower than 50 Pa is less than 5 ppm at both $L_s = 110°$ and 150°. Whatever the discrepancy nearer the surface, the models do not appear to resolve the higher altitude clouds that are unambiguously observed.

[16] *Hinson and Wilson* [2004] and *Lee et al.* [2009] argue that the water ice distribution is controlled by the thermal tides. Water ice condenses if the water vapor partial pressure is greater than the saturation pressure of water vapor with respect to ice (and sufficient nuclei are available). Since the saturation pressure of water vapor is a strong function of temperature, water ice will tend to condense near temperature minima such as the anti-nodes of the diurnal tide. As these anti-nodes vertically propagate in the atmosphere during the course of the day, the clouds associated with them should evaporate and re-condense in phase with the propagation of the tide. Figures 2d and 2h support this hypothesis very clearly, since the tropical water ice layer on the dayside (nightside) is at a level of the atmosphere that is warmer during the night (day) than during the day (night). Thus, a layer of high q_{ice} moves up and down with the thermal tide during late summer.

[17] Equations (1) and (2) permit a calculation of the infrared heating due to such a layer, using the water ice radiative parameters of the broadband model of *Hinson and Wilson* [2004]. The ice grain size assumed in this model (4 μm) is larger than assumed by the retrieval algorithm. Since lowering the grain size significantly lowers the single scattering albedo at all wavelengths, this estimate should be a lower bound. We assume: T_s=263 K (day) and 197 K (night) [*Schofield et al.*, 1997]; T_e=165 K (day) and 145 K (night); and c_p=756 J kg^{-1}. In this case, the daytime heating rate is

2.1 K sol^{-1} ppm^{-1} and the nighttime heating rate is 0.4 K sol^{-1} ppm^{-1}. The zonal average tropical diabatic heating at northern summer solstice was estimated to range from −10 to 10 K sol^{-1} in a GCM simulation without aerosol by *Medvedev and Hartogh* [2007], so a zonal average 10–20 ppm water ice cloud in the tropics should produce diabatic heating comparable to that of gaseous absorbers and thus perturb the circulation. In addition, the heating due to the high q_{ice}, longitudinally scattered clouds in Figure 3b–3d could be a significant asymmetric forcing.

[18] The most significant difference between the water ice cloud observations presented here and published model results is the level at which water ice clouds are found. *Rind and Rossow* [1984] observe that circulations are perturbed toward a thermally direct state at a given pressure level if the equator to pole temperature gradient is positive. Thus, neglecting eddy terms, radiative heating by water ice may drive a thermally direct circulation like the Hadley cell on the Earth that effectively becomes part of the equivalent to the Hadley cell on Mars: the principal meridional overturning cell (PMOC). The higher the clouds, the deeper the cell. Therefore, the PMOC during northern summer may be stronger at higher altitudes than simulated by both the published models that simulate water ice clouds and by models that do not simulate such clouds. If the upwelling of the PMOC controls the tropical water vapor distribution [*Richardson et al.*, 2002; *Richardson and Wilson*, 2002], water ice clouds also could have a positive feedback (mainly limited by the water vapor supply) on the PMOC's height and intensity.

References

Benson, J. L., D. M. Kass, A. Kleinböhl, D. J. McCleese, J. T. Schofield, and F. W. Taylor (2010), Mars' south polar hood as observed by the Mars Climate Sounder, *J. Geophys. Res.*, doi:10.1029/2009JE003554, in press.

Clancy, R. T., B. J. Sandor, M. J. Wolff, P. R. Christensen, M. D. Smith, J. C. Pearl, B. J. Conrath, and R. J. Wilson (2000), An intercomparison of ground-based millimeter, MGS TES, and Viking atmospheric temperature measurements: Seasonal and interannual variability of temperatures and dust loading in the global Mars atmosphere, *J. Geophys. Res.*, 105(E4), 9553–9571, doi:10.1029/1999JE001089.

Hinson, D. P., and R. J. Wilson (2004), Temperature inversions, thermal tides, and water ice clouds in the Martian tropics, *J. Geophys. Res.*, 109, E01002, doi:10.1029/2003JE002129.

Kleinböhl, A., et al. (2009), Mars Climate Sounder limb profile retrieval of atmospheric temperature, pressure, dust, and water ice opacity, *J. Geophys. Res.*, 114, E10006, doi:10.1029/2009JE003358.

Lee, C., et al. (2009), Thermal tides in the Martian middle atmosphere as seen by the Mars Climate Sounder, *J. Geophys. Res.*, 114, E03005, doi:10.1029/2008JE003285.

McCleese, D. J., J. T. Schofield, F. W. Taylor, S. B. Calcutt, M. C. Foote, D. M. Kass, C. B. Leovy, D. A. Paige, P. L. Read, and R. W. Zurek (2007), Mars Climate Sounder: An investigation of thermal and water vapor structure, dust and condensate distributions in the atmosphere, and energy balance of the polar regions, *J. Geophys. Res.*, 112, E05S06, doi:10.1029/2006JE002790.

Medvedev, A. S., and P. Hartogh (2007), Winter polar warmings and the meridional transport on Mars simulated with a general circulation model, *Icarus*, 186(1), 97–110, doi:10.1016/j.icarus.2006.08.020.

Montmessin, F., F. Forget, P. Rannou, M. Cabane, and R. M. Haberle (2004), Origin and role of water ice clouds in the Martian water cycle as inferred from a general circulation model, *J. Geophys. Res.*, 109, E10004, doi:10.1029/2004JE002284.

Nelli, S. M., J. R. Murphy, W. C. Feldman, and J. R. Schaeffer (2009), Characterization of the nighttime low-latitude water ice deposits in the NASA Ames Mars General Circulation Model 2.1 under present-day atmospheric conditions, *J. Geophys. Res.*, 114, E11003, doi:10.1029/2008JE003289.

Richardson, M. I., and R. J. Wilson (2002), Investigation of the nature and stability of the Martian seasonal water cycle with a general circulation model, *J. Geophys. Res.*, 107(E5), 5031, doi:10.1029/2001JE001536.

Richardson, M. I., R. J. Wilson, and A. V. Rodin (2002), Water ice clouds in the Martian atmosphere: General circulation model experiments with a simple cloud scheme, *J. Geophys. Res.*, 107(E9), 5064, doi:10.1029/2001JE001804.

Rind, D., and W. B. Rossow (1984), The effects of physical processes on Hadley circulation, *J. Atmos. Sci.*, 41, 479–507, doi:10.1175/1520-0469(1984)041<0479:TEOPPO>2.0.CO;2.

Schofield, J. T., J. R. Barnes, D. Crisp, R. M. Haberle, S. Larsen, J. A. Magalhães, J. R. Murphy, A. Seiff, and G. Wilson (1997), The Mars Pathfinder Atmospheric Structure Investigation/Meteorology (ASI/MET) experiment, *Science*, 278, 1752–1758, doi:10.1126/science.278.5344.1752.

Smith, M. D. (2004), Interannual variability in TES atmospheric observations of Mars during 1999–2003, *Icarus*, 167, 148–165, doi:10.1016/j.icarus.2003.09.010.

Spiga, A., and F. Forget (2009), A new model to simulate the Martian mesoscale and microscale atmospheric circulation: Validation and first results, *J. Geophys. Res.*, 114, E02009, doi:10.1029/2008JE003242.

Wang, H., and A. P. Ingersoll (2002), Martian clouds observed by Mars Global Surveyor Mars Orbiter Camera, *J. Geophys. Res.*, 107(E10), 5078, doi:10.1029/2001JE001815.

Wilson, R. J., G. A. Neumann, and M. D. Smith (2007), Diurnal variation and radiative influence of Martian water ice clouds, *Geophys. Res. Lett.*, 34, L02710, doi:10.1029/2006GL027976.

Wilson, R. J., S. R. Lewis, L. Montabone, and M. D. Smith (2008), Influence of water ice clouds on Martian tropical atmospheric temperatures, *Geophys. Res. Lett.*, 35, L07202, doi:10.1029/2007GL032405.

W. A. Abdou, J. L. Benson, D. M. Kass, A. Kleinböhl, D. J. McCleese, J. T. Schofield, J. H. Shirley, and P. M. Wolkenberg, Jet Propulsion Laboratory, California Institute of Technology, 4800 Oak Grove Dr., Pasadena, CA 91109, USA.

N. G. Heavens, Department of Earth and Atmospheric Sciences, Cornell University, 1118 Bradfield Hall, Ithaca, NY 14850, USA. (heavens@cornell.edu)

M. I. Richardson, Ashima Research, 600 S. Lake Ave., Ste. 303, Pasadena, CA 91106, USA.